

Math. Model. Nat. Phenom.
 Vol. 12, No. 4, 2017, pp. 108–123
 DOI: 10.1051/mmnp/201712409

Noise Enhanced Signaling in STDP Driven Spiking-Neuron Network

S.A. Lobov^{1*}, M.O. Zhuravlev¹, V.A. Makarov^{1,2**}, V.B. Kazantsev¹

¹Lobachevsky State University of Nizhny Novgorod, Gagarin Ave. 23, 603950 Nizhny Novgorod, Russia

²Instituto de Matemática Interdisciplinar, Dept. de Matemática Aplicada, Universidad Complutense de Madrid, Avda Complutense s/n, 28040 Madrid, Spain

Abstract. Population spike signaling is widely observed both in intact brain and neuronal cultures. Experimental evidence suggests that a locally applied electrical stimulus can shape the network architecture and thus the neuronal response. However, there is no clue on how this process can be controlled. Here we study a realistic model of a culture of cortical-like neurons with spike timing dependent plasticity. We show that a stimulus applied at a corner of the culture can rebuild synaptic couplings. Then the network eventually switches from a turbulent-like asynchronous spiking to an ordered population spike signaling mode. The structural analysis shows that the stimulus potentiates centrifugal couplings, which promotes spiking waves traveling outwards the stimulus location. This phenomenon can be catalyzed by noise of an intermediate strength. We predict that matured cultures with high connectivity are more susceptible to reconfiguration and generation of a population spike response than young cultures with low connectivity. We also report on an intermittent synchronization causing switches between two quasi-stable states: generation of time-locked population spikes and turbulent spiking. In the turbulent mode the stimulus excites patches of spiking activity randomly traveling in the network. Such a regime can be implemented through a large scale looping of couplings backwards to the stimulus location. We anticipate that the robust mechanisms of shaping the network architecture discussed here can also be effective in more complex preparations and studies of the relationship between network structure and function.

Keywords and phrases: spiking neuron network, forced synchronization, synaptic modulation, stochastic resonance

Mathematics Subject Classification: 92B25, 92B20, 37H10, 37B55

1. Introduction

A great variety of large-scale brain networks are assembled from spiking neurons that use population spikes for coding and transferring information among distant nuclei. Sensible examples can be found, e.g., in the hippocampal CA3 – CA1 pathways [15, 23]. In particular, recent experimental evidence suggests that population signaling between left and right hippocampal lobes is asymmetric [3]. Bilateral excitation is

*Corresponding author. E-mail: lobov@neuro.nnov.ru

**Corresponding author. E-mail: vmakarov@ucm.es

generally led by the right hemisphere, which promotes lateralized synchronization of gamma strings for optimal convergence on CA1 targets.

In *in vitro* studies similar but simplified spiking signaling can be studied in preparations of dissociated neuronal cultures [13, 20, 33]. Under neural development such cultures can exhibit formation of well-organized spontaneous bursts that involve spiking of almost all neurons in the culture [37]. The burst frequency increases with the culture age from 0.01 Hz for day 3 to 0.5 Hz for day 40 [20]. The synaptic architecture formed during development shapes the spatiotemporal properties of the bursts [20, 26]. Although the bursting activity in a developed culture can exhibit strong variability [37], there may also exist the so-called spiking “signatures”, i.e., stable patterns of spikes repeating from burst to burst [26].

Relatively recently there have appeared attempts to use cultures of spiking neurons as decision-making ganglia driving mobile robots, the so-called neuroanimats (see, e.g., [2, 10, 30]). The sensory information on the presence of an obstacle located on the right or left hand side of a neuroanimate stimulates a neuronal culture and provokes population bursts with different spiking signatures [30]. Then the neuroanimate detects and classifies spiking burst and moves in the corresponding direction. Bakkum and colleagues [2] claim that a neuroanimat after few minutes of “training” is capable of moving in a desired direction within 30° corridor. Nevertheless, at the moment there is no effective training protocol for shaping the architecture and function of cultures. The high variability of bursting patterns in spontaneously formed neural networks impedes controlling the whole network activity under local stimulation.

Thus, the use of mathematical models describing the dynamics of large-scale realistic neural networks is a convenient tool for studying the biophysical mechanisms behind plastic changes, formation of network structures, and population bursts [7, 21, 28]. Known biologically relevant models of neuronal cultures incorporate synaptic plasticity and can form different connectivity patterns mimicking different stages of neural development (see, e.g., [8, 18, 28]). It has been shown that leaky integrate and fire models with adequate spike-timing-dependent plasticity (STDP) can exhibit population bursts quite similar to those observed experimentally [8]. Kawasaki and colleagues [18] showed that the burst shape and timing can be explained by a model that includes closed-loop neurite outgrowth and dynamic synapses. Numerical simulations of cultures with pacemakers confirmed that such neurons regularize the shape and duration of bursts [11, 12].

One of the open fundamental questions is the possibility to shape the response of a neuronal culture to specific external stimuli. It was shown that random background stimulation may help maintaining the synaptic architecture after tetanization [8]. Recently, an evidence that local electric stimulation can lead to generation of population bursts synchronized with the stimulus has been provided [19]. Such bursts can be observed under a periodic stimulation. Then the neural plasticity expands the frequency range of the stimulus evoking synchronous bursts. However, the problem of controlling the population spiking activity by a single electrode stimulation remains largely unsolved.

Another significant issue that has received less attention in the literature is the influence of an internal noise on the population spike signaling. Earlier it was widely demonstrated that noise may crucially affect the behavior of different dynamical systems (for review see, e.g, [1]). In particular, it can provoke a stochastic resonance, i.e., noise of an intermediate intensity can increase the coherence of the system response to external stimuli [5, 24]. We foresee that such an effect may enhance the formation of signaling pathways in a neural culture and thus improve its information processing abilities.

In this work we study a mathematical model of a neuronal culture under a local (single electrode) periodic electrical stimulation. The network model includes excitatory and inhibitory spiking neurons driven by an intrinsic noise and interneuronal couplings undergo STDP. We show that the noise of an intermediate intensity can significantly enhance the burst synchronization. Then all neurons in the network fire spikes synchronized with the periodic stimulus. The noise intensity facilitating the synchronized response depends on the network connectivity: the stronger the connectivity, the smaller the noise intensity is required for synchronization. In other words, the connectivity index plays the role of noise. We also show that in certain cases the network may exhibit a complex intermittent behavior. Time intervals of fully

synchronous spiking responses swap with intervals of partial synchronization. Such a behavior may be useful for building next-generation neuroanimats.

2. Model of *in vitro* neural network

To model a neuronal culture we implement a neural network consisting of 400 excitatory and 100 inhibitory cells randomly distributed over a (1.2×1.2) mm square substrate (Fig. 1A). Each neuron in average can receive synaptic inputs from $N^v = 15$ to 80 cells randomly selected from its neighborhood. The order of each vertex in the neuronal graph, N_i^v , is taken from a Gaussian distribution $N_i^v \sim \mathcal{N}(N^v, 0.1N^v)$. Then N_i^v edges (couplings) are distributed among nearest neurons with the probability decaying with the distance between the neuron and its targets. Such a network geometry (3–15% interneuron couplings) resembles typical connectivity structure observed in *in vitro* experiments with dissociated cultures of cortical neurons [22] and it was widely used in numerical simulation [7, 8].

To describe the dynamics of each individual neuron we employ the Izhikevich model, known to reproduce a variety of neuronal behaviors whilst being computationally efficient [17]:

$$\begin{aligned} \frac{dv_i}{dt} &= 0.04v_i^2 + 5v_i + 140 - u_i + \xi_i(t) + I_i(t), \\ \frac{du_i}{dt} &= a(bv_i - u_i), \end{aligned} \quad (2.1)$$

where v_i is the membrane potential and u_i is the recovery variable. The model is assumed to emit a spike if the membrane potential reaches a threshold. Then, the state variables are reset according to

$$\text{if } v_i \geq 30 \text{ mV, then } v_i \leftarrow -65, \quad u_i \leftarrow u_i + 8. \quad (2.2)$$

In numerical simulations we set $a = 0.02$ and $b = 0.2$, which corresponds to a silence regime in the absence of external drive and to a regular spiking mode under the influence of a constant current [17]. Such a behavior is the most typical for cortical pyramidal neurons.

In Eq. (2.1) the term $\xi_i(t)$ models an uncorrelated zero-mean white Gaussian noise with variance D , i.e., $\langle \xi_i(t) \rangle = 0$ and $\langle \xi_i(t)\xi_j(t') \rangle = D\delta_{ij}\delta(t-t')$, where δ is the Kronecker’s symbol. The external current $I_i(t)$ describes the compound input from presynaptic neurons and external stimulus

$$I_i(t) = I_i^{\text{syn}}(t) + I_i^{\text{stiml}}(t). \quad (2.3)$$

The stimulus, $I_i^{\text{stiml}}(t)$, is a sequence of square electrical pulses of duration 3 ms delivered at 10 Hz (Figs. 1A and 1B). We apply the stimulating current locally in a corner of the culture to a small group of neurons consisting of one inhibitory and five excitatory neurons. The current magnitude is selected in such a way that it will be enough to excite the stimulated neurons.

The synaptic current is given by the weighted sum of the outputs of presynaptic neurons

$$I_i^{\text{syn}}(t) = \sum_j g_j w_{ij} y_{ij}(t), \quad (2.4)$$

where the sum is taken over all presynaptic neurons, $w_{ij} \in [0, 1]$ is the strength of the synaptic coupling directed from neuron j to i , g_j is the scaling factor equal either to 20 or -20 for excitatory and inhibitory neurons, respectively, and $y_{ij}(t)$ describes the amount of neurotransmitters released by presynaptic neuron j .

To model the neurotransmitters we use the Tsodyks-Markram’s equations [32] that account for short-term depression and facilitation

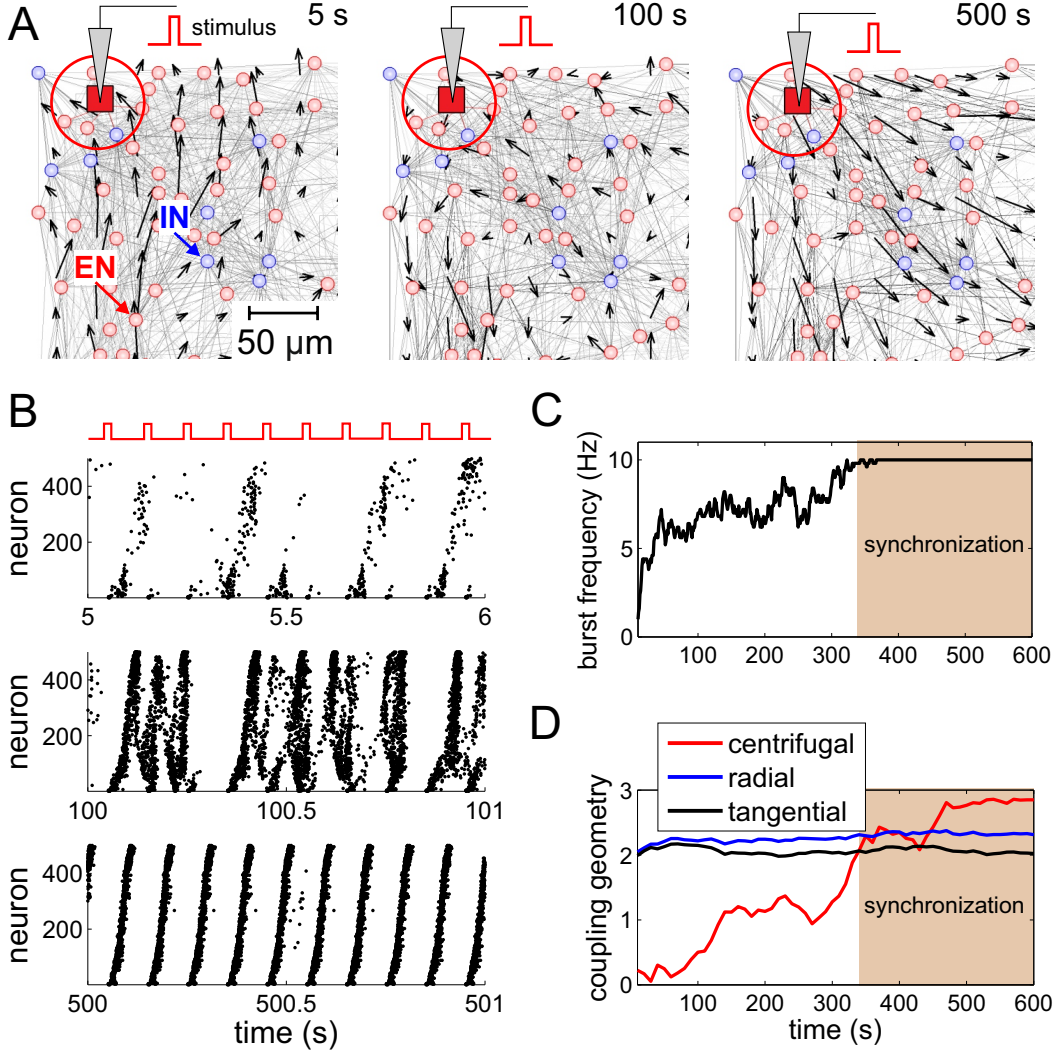


FIGURE 1. Modeling the population spike signaling in a dissociated neural culture: network architecture and function. A) Three examples of a small part of the neural network near the “stimulus electrode” (big red circle). Panels correspond to the beginning of the stimulation, $t = 5$ s, intermediate time, $t = 100$ s, and mature network, $t = 500$ s. Small red and blue circles mark positions of the excitatory (EN) and inhibitory (IN) neurons, respectively. Gray lines mark interneuron couplings. Black arrows show the connectivity vector field (see main text). B) Traces of external stimuli (top, in red) and raster displays of the spiking activity in the network corresponding to different behaviors: no population bursting, intermittent bursting, and population spikes time-locked with the stimulus. Neurons were previously ordered by their distance to the stimulus center p_{st} . C) Frequency of the population burst. D) Dynamics of the coupling geometry indexes.

$$\begin{aligned}
 \frac{dx_{ij}}{dt} &= \frac{z_{ij}}{\tau_{rec}} - q_{ij}^+ x_{ij}^- \delta(t - t_j - \tau_{ij}), \\
 \frac{dy_{ij}}{dt} &= -\frac{y_{ij}}{\tau_I} + q_{ij}^+ x_{ij}^- \delta(t - t_j - \tau_{ij}), \\
 \frac{dz_{ij}}{dt} &= \frac{y_{ij}}{\tau_I} - \frac{z_{ij}}{\tau_{rec}}, \\
 \frac{dq_{ij}}{dt} &= -\frac{q_{ij}}{\tau_{facil}} + \frac{1}{2}(1 - q_{ij}^-) \delta(t - t_j - \tau_{ij}),
 \end{aligned} \tag{2.5}$$

where x_{ij} , y_{ij} , and z_{ij} are the fractions of synaptic resources (neurotransmitters) in the recovered, active, and inactive states, respectively, q_{ij} describes the effective use of synaptic resources, t_j is the time of occurrence of a presynaptic spike, $\tau_I = 10$ ms is the decay constant of post synaptic currents, $\tau_{\text{rec}} = 50$ ms is the recovery time from synaptic depression.

In Eq. (2.5) we take into account the time delay of spike transmission between neurons i and j

$$\tau_{ij} = \frac{d_{ij}}{V}, \quad (2.6)$$

where d_{ij} is the linear distance between the neurons and $V = 0.05$ m/s is the spike transmission velocity. The maximal possible delay corresponding to a link between the diagonal corners of the substrate is 34 ms, however, such long links are highly improbable in our model. The notation q^- (q^+) in (2.5) indicates that the value of q is taken just before (after) the resetting instant in (2.2) caused by arrival of a presynaptic spike. The synaptic efficacy, q_{ij} , increases with each presynaptic spike and decays to the zero baseline with the time constant $\tau_{\text{facil}} = 1$ s.

The synaptic weights of the excitatory neurons, w_{ij} , are governed by an STDP implemented with two local variables [25, 31]. A presynaptic spike at t_j induces a weight decrease proportional to the value of the postsynaptic trace s_i . Similarly, a postsynaptic spike at t_i induces a weight potentiation proportional to the value of the presynaptic trace s_j

$$\begin{aligned} \frac{ds_i}{dt} &= -\frac{s_i}{\tau_i} + \sum_{t_i} \delta(t - t_i), \\ \frac{ds_j}{dt} &= -\frac{s_j}{\tau_j} + \sum_{t_j} \delta(t - t_j - \tau_{ij}), \\ \frac{dw_{ij}}{dt} &= F_l(w_{ij})s_j\delta(t - t_i) - F_a(w_{ij})s_i\delta(t - t_j - \tau_{ij}), \end{aligned} \quad (2.7)$$

where $\tau_i = 10$ ms and $\tau_j = 10$ ms are the corresponding time constants. The weighting functions obey the multiplicative updating rule [14, 25]:

$$F_l(w_{ij}) = \lambda(1 - w_{ij}), \quad F_a(w_{ij}) = \lambda\alpha w_{ij}, \quad (2.8)$$

where $\lambda = 0.001$ is the learning rate and $\alpha = 5$ is the asymmetry parameter.

At the beginning the synaptic weights $w_{ij}(t = 0)$ are taken from a Gaussian distribution $\mathcal{N}(0.5, 0.1)$, i.e., the initial weights are medial and similar over the network. Then the network is integrated up to $t = 10^6$ s without external stimulation. This corresponds to settling the network by a spontaneous activity used in experimental protocols. After that we apply periodic stimulation and study the network response. Further on, all given times are related to the beginning of the stimulation epoch.

3. Structural connectivity changes and population spikes induced by local stimulus

Following typical experimental protocol [8, 26] we apply an external stimulus (short square pulses) to a small group of neighboring cells located in a corner of the modeled culture (Fig. 1A, big red circle). Such a simulation mimics local one-electrode electrical stimulation applied to a dissociated culture grown on a multi-electrode array. The stimulus driven neurons fire spikes synchronized with the stimulus. Further the activation can spread in the network, which finally can induce a population spike (Fig. 1B).

The spreading of excitation in the network induces STDP. To monitor the plastic changes in the network we study the spatial distribution of the synaptic weights (w_{ij}). To describe it on a large-scale we evaluate the connectivity vector field [19]. The square substrate covered by the network is divided into a 24×24 grid consisting of 576 cells. A link going from neurons i to j located at \mathbf{p}_i and \mathbf{p}_j ($\mathbf{p}_i, \mathbf{p}_j \in \mathbb{R}^2$)

is represented as a vector directed from the presynaptic to postsynaptic neuron with the length equal to the corresponding coupling weight

$$\mathbf{c}_{ij} = w_{ij} \frac{\mathbf{p}_i - \mathbf{p}_j}{\|\mathbf{p}_i - \mathbf{p}_j\|_2}. \quad (3.1)$$

All vectors passing through cell (k, l) in the grid are added and we get the resulting vector for the given cell

$$\mathbf{C}_{kl} = \sum_{ij \in \Lambda_{kl}} \mathbf{c}_{ij}, \quad (3.2)$$

where Λ_{kl} is the set of vectors having nonempty intersection with cell (k, l) . Then the matrix $(\mathbf{C}_{kl}) \in \mathcal{M}_{24 \times 24}(\mathbb{R}^2)$ defines the large-scale connectivity vector field. Note that since $w_{ij} = w_{ij}(t)$, the field (3.2) can change in time.

Figure 1A (black arrows) shows examples of the vector field. The field describes the average connectivity among (24×24) network areas and helps visualizing the direction of propagation of the excitation in the network. We also can monitor changes in the neural architecture induced by STDP. At the beginning the synaptic connections are mostly directed towards the stimulated neurons (Fig. 1A, $t = 5$ s). Thus, there are no strong connections going from the stimulator to the network. Therefore, the stimulus evoked excitation hardly propagates outside and no synchronous network response is observed (Fig. 1B, $t = 5$ s). Then STDP starts reshaping the links in the neighborhood of the stimulus location. The coupling directed towards the stimulus area decay and those that go outwards are strengthened. Such a change in the network geometry facilitates radial propagation of excitation, which becomes dominating (Figs. 1A and 1B, $t = 100$ and 500 s).

To get a global insight into the structure of network couplings we introduce three measures: centrifugal, radial, and tangential indexes. To evaluate them let $\{\mathbf{p}_i^{\text{st}}\}_{i=1}^5$ be the positions of the stimulus driven neurons. Then we define the stimulus center

$$\mathbf{p}_{\text{st}} = \frac{1}{5} \sum_{i=1}^5 \mathbf{p}_i^{\text{st}}. \quad (3.3)$$

To evaluate the centrifugal index we calculate the dot-product of all vectors \mathbf{c}_{ij} describing the interneuron couplings with the vectors formed by the positions of neurons and the stimulus center

$$\mathcal{C} = 2 \sum_{ij} \langle \mathbf{c}_{ij}, \mathbf{r}_i \rangle, \quad \mathbf{r}_i = \frac{\mathbf{p}_i - \mathbf{p}_{\text{st}}}{\|\mathbf{p}_i - \mathbf{p}_{\text{st}}\|_2}. \quad (3.4)$$

This index can be either positive or negative. High positive (negative) values correspond to prevalence of centrifugal (centripetal) couplings related to the stimulus center, whereas a value closed to zero means the absence of a favorite radial direction. Then the radial index is constructed in a similar way but it operates over absolute values

$$\mathcal{R} = \sum_{ij} |\langle \mathbf{c}_{ij}, \mathbf{r}_i \rangle|. \quad (3.5)$$

This index allows estimating potentiation/depression of the radially directed couplings without paying attention to their direction (centrifugal or centripetal). Finally the tangential index evaluates the coupling density in the direction orthogonal to the radial vectors \mathbf{r}_i^\perp ($\langle \mathbf{r}_i^\perp, \mathbf{r}_i \rangle = 0$, $\|\mathbf{r}_i^\perp\|_2 = 1$)

$$\mathcal{T} = \sum_{ij} |\langle \mathbf{c}_{ij}, \mathbf{r}_i^\perp \rangle|. \quad (3.6)$$

The adaptive reorganization in the network structure above discussed leads to a change in network function (Fig. 1B). To describe the functional changes in the network we introduce the spiking rate

$$S(t) = \frac{1}{N\Delta} \sum_{i=1}^N n_i(t; \Delta) \quad (3.7)$$

where N is the total number of neurons and $n_i(t; \Delta)$ is the number of spikes emitted by neuron i in time interval $[t, t + \Delta)$, where $\Delta = 50$ ms. The spiking rate close to zero indicates slow network firing corresponding to spontaneous activity, whereas $S(t)$ close to 1 indicates massive synchronized firing in the network. We then aim at detecting population spikes synchronized with the stimulus. Thus, we introduce the population spike frequency by the following way

$$F(t) = \frac{1}{2T} \int_{t-T}^t \delta(S(z) - S_{\text{thr}}) dz \quad (3.8)$$

where $T = 5$ s is the averaging period and $S_{\text{thr}} = 1/4$ is the threshold determining the beginning of a population spike. The function $F(t)$ evaluates the mean frequency of population spikes. Thus, the values of $F(t)$ close to the stimulus frequency (10 Hz) indicate synchronous spiking response of the network to each stimulus event. Otherwise we conclude on asynchronous spiking behavior.

Figure 1C shows the time evolution of the frequency of population spikes. At the beginning the network structure does not favor propagation of excitation in the network and we observe low values of F . Then STDP shapes the couplings and make the network structure more regular, which facilitates excitation of a traveling wave. Indeed, at $t > 340$ s $F(t)$ reaches the value of 10 Hz and each stimulus event is accompanied by a time-locked population spike that engages practically all neurons in the network (Fig. 1B, $t = 500$ s).

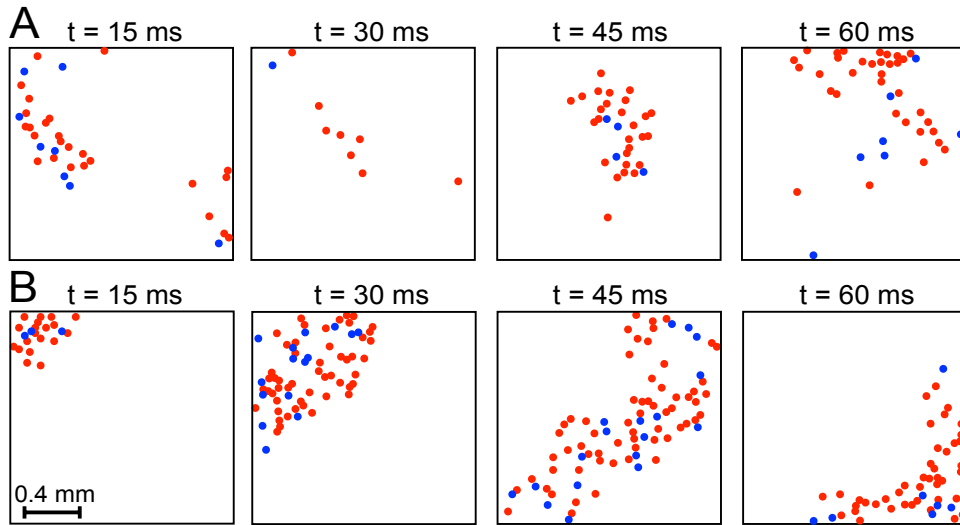


FIGURE 2. Propagation of excitation in an unstructured (A) and structured (B) neural networks. Red and blue dots mark excitatory and inhibitory neurons, respectively, excited within 5 ms time interval.

In raster plots shown in Fig. 1B we ordered neurons by their distance to the stimulus center \mathbf{p}_{st} . Thus, the inclined traces of population spikes at $t = 500$ s suggest traveling waves starting from the stimulus location and propagating outwards. It is known that waves can propagate in structured neural networks, whereas random couplings can destroy them. Thus, we hypothesize that STDP under stimulation reshapes the network and facilitates traveling waves.

To validate this hypothesis we evaluated the connectivity indexes $\mathcal{C}(t)$, $\mathcal{R}(t)$, and $\mathcal{T}(t)$ [Eqs. (3.4)-(3.6)]. Figure 1D shows their time evolution. The radial and tangential indexes do not suffer strong changes, while the centrifugal index grows strongly. This means that in average the network maintains its structure established during the spontaneous activity. However, we also observe a simultaneous decrease of

centripetal and increase of centrifugal couplings. Such a network reshaping enables the wave propagation. Figure 2 shows consecutive snapshots of the network response to a stimulus event at the beginning of stimulation (A) and after the end of the network reshaping process (B). Indeed, at the beginning only patches of excited neurons can be observed. These patches have no clear propagation direction due to unstructured couplings in the network. However, after 500 s we get a robust traveling wave starting at the stimulus location (upper-left corner) and propagating outwards. The wave engages practically all neurons and we thus observe clear population spike.

Thus, population spike signaling occurs due to reshaping the network from an unstructured to the centrifugal form.

4. Stochastic resonance synchronization of network response with stimulus

The model (2.1) includes noisy forces that may influence both the structural and functional properties of the neural network. Let us now study how noise affects the dynamics, i.e., the function of the neural network.

We fix the vertex order at $N^v = 20$, which is within the experimental interval observed in dissociated neuronal cultures. Then we run simulations with different values of the noise intensity. Figure 3A shows five examples of the time evolution of the frequency, $F(t)$, obtained for progressively increasing noise magnitudes. At low noise intensity (Fig. 3A, $D = 0.3$) no population spike is generated and hence $F(t)$ is close to zero. By increasing the noise strength to $D = 1.5$ we achieve a sudden synchronization of the network activity, which leads to generation of population spikes synchronized with the stimulus (similar to Fig. 1B). However, this synchronous regime disappears after few hundred seconds. It reappears again after some transient time and then the process repeats. Thus, we observe an intermittent network synchronization and generation of population spikes time-locked to the stimulus and this regime eventually switches back to network “silence”. Such an intermittent behavior is quite typical for forced nonlinear dynamical systems near the boundary of synchronization [4, 27].

At intermediate noise intensity, $D = 4.5$, we achieve full and persistent in time synchronization of the network activity with the stimulus (Fig. 3A). Further increasing of the noise strength leads first to intermittent synchronization ($D = 8$) and then to a noise driven oscillation with no role of the stimulus ($D = 9$).

Thus, we observe a special type of the stochastic resonance phenomenon. The population spiking response of the network can fully synchronize to the stimulus at intermediate noise intensities, while synchronization is destroyed at small and big noise magnitudes. To cross-check our finding we repeated the calculations for 20 different noise values and evaluated the synchronization index as the inverse time required to achieve the first synchronization epoch, i.e., $|F(t) - 10| \leq 0.5$ Hz for $t \in [T^*, T^* + 10]$ s

$$S_{\text{sync}} = \frac{1}{T^*} \quad (4.1)$$

Figure 3B shows the synchronization index *vs* the noise strength. Indeed, there is an interval of the noise level that results in either full or intermittent synchronization. Note that switching between no synchronous and synchronous modes occurs through a sharp jump. Depending on experiment the jump occurs at different noise intensity in the interval marked by gray stripe in Fig. 3B.

To explain the basic mechanism underlying noise enhanced synchronization let us consider a small network of three interconnected neurons (Fig. 3C, before stimulation). Neuron 1 receives stimulus input and thus generates spike for each stimulus event. Spikes from the 1st neuron further excite neurons 2 and 3 along centrifugal couplings. At $t = 0$ all synaptic couplings are low enough hence presynaptic spikes cannot fire neurons 2 and 3. Then we simulated the network with three different values of the noise intensities.

In the case of low noise (Fig. 3C, low noise) neurons 2 and 3 stay far from the excitation threshold and generate seldom spikes. These spontaneous spikes are not correlated with the spiking activity of neuron 1 and hence STDP does not alter the coupling strengths and they remain small. Thus, no population

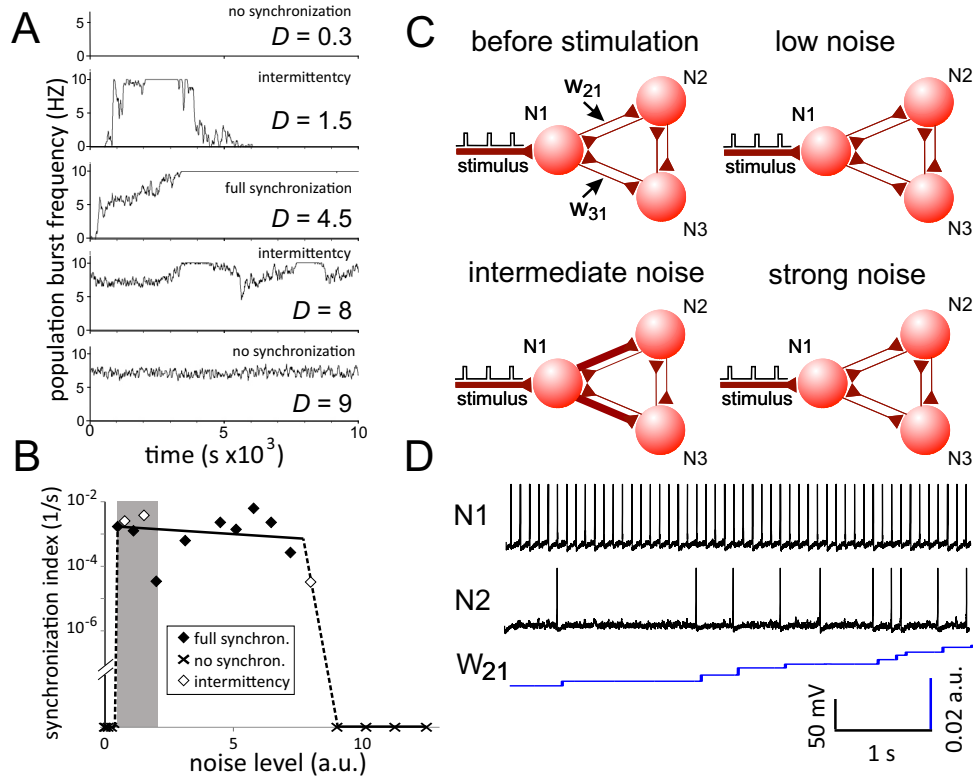


FIGURE 3. Stochastic resonance in neural networks driven by periodic stimulus. A) Five examples of the time evolution of the frequency of population spikes, $F(t)$, for different noise intensities D . By increasing the noise intensity the network response goes from no synchronization to intermittent and full synchrony and then returns to no synchronization through intermittent behavior (the vertex order $N^v = 20$). B) The synchronization index, S_{sync} , vs. noise intensity, D , exhibits a typical peak at intermediate noise intensity ($N^v = 20$). Grey stripe indicates the interval of noise intensities corresponding to appearance of synchronization for different networks ($n = 8$). C) Three neuron network illustrating the phenomenon of stochastic resonance. D) Time evolution of the spiking activity of neurons N1 and N2 and the interneuron coupling w_{21} at an intermediate noise level.

spike can be generated in this situation. For the intermediate noise intensity (Fig. 3C, intermediate noise) neurons 2 and 3 are closer to the spiking threshold. This helps the weak excitatory postsynaptic potentials generating spikes correlated with the presynaptic spikes. Figure 3D illustrates the spiking activity of neurons 1 and 2, and the time evolution of the centrifugal coupling w_{21} in this case. Indeed, due to noise neuron 2 starts firing spikes correlated with the presynaptic input, which leads to increasing steps in w_{21} . Higher coupling, in turn, facilitates response of neuron 2 synchronous with the stimulus. The same process happens with neuron 3. Thus, after a transient all tree neurons in the network generate population spikes time-locked to the stimulus events. In the case of strong noise (Fig. 3C, strong noise) neurons 2 and 3 generate many spontaneous spikes uncorrelated with firing of neuron 1. This leads to depression of connections and hence to a lack of the synchronous dynamics. Thus, noise can help reshaping the network to the centrifugal structure and this facilitates population spike signaling.

In terms of neuronal cultures the vertex order, N^v , resembles different stages of the neural development from young (low connectivity) to mature (high connectivity) states. Let us now study how the coupling density influences the stochastic resonance behavior. Figure 4A shows the results of simulations

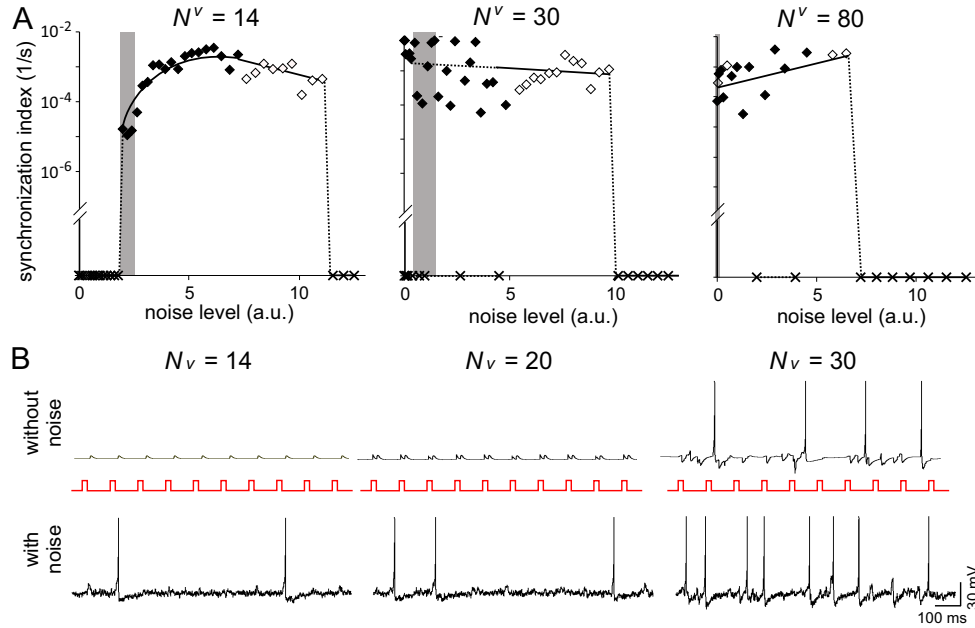


FIGURE 4. The connectivity index plays the role of noise and facilitates synchronization. A) The synchronization index, S_{sync} , vs. noise intensity, D , for networks with different connectivity index, N^v (see also, Fig. 3B). Gray stripes indicate the variability of the synchronization threshold ($n = 8$). B) Membrane potential, v_i , recorded from a neuron located rather far from the stimulus location for different network connectivity values without (top) and with (bottom) noise. At high enough connectivity the network input to the neuron plays the role of noise and excites it, thus promoting population spikes.

of networks with different vertex orders. In the case of low connectivity (Fig. 4A, $N^v = 14$ and Fig. 3B, $N^v = 20$) we get stable correspondence between the synchronization index and noise level, typical for the stochastic resonance phenomenon. For higher connectivity (Fig. 4A, $N^v = 30, 80$) the synchronization index becomes bistable. For the same noise intensity the synchronous mode can be either achieved or not on extremely long time intervals ($> 10^6$ s). Another interesting observation is that the higher connectivity the lower noise intensity is required for switching to synchronous mode (Fig. 4A, $N^v = 14$ vs. $N^v = 30$). Moreover, at high enough connectivity the network response synchronizes to the stimulus without noise (Fig. 4A, $N^v = 80$). In this case, the connectivity order plays the role of noise. A large number of connections receiving by a given neuron provoke chaotic and high enough synaptic current similar to the stochastic perturbation induced by noise.

To illustrate this effect we select a neuron located far enough from the stimulus location. Then the signal transmission to this neuron is polysynaptic, i.e., the excitation comes via different pathways with different overall conduction delays. As we discussed above noise promotes excitation of neurons. Thus, in general in the presence of noise we observe higher spiking activity (Fig. 4B, top vs. bottom rows). Moreover, higher spontaneous spiking activity increases the probability of generation of spikes correlated with the stimulus, which leads to a reorganization of the network to a centrifugal oriented structure. This finally promotes population spikes. In this context the connectivity index N^v plays the role of noise. Even in the absence of noise the high number of polysynaptic connections (Fig. 4B, $N^v = 30$) may serve as a substrate enhancing the correlation of spikes to the stimulus. This phenomenon explains the shift of the lower threshold of the noise intensity required for synchronization to lower values of the noise strength (Fig. 4A).

Thus, we can conclude that mature networks are propitious to full synchronization and generation of population spikes time-locked to the stimulus.

5. Intermittent synchronization of population spike with stimulus

Above we observed that for a certain noise magnitude the network can synchronize with the stimulus in an intermittent regime (Fig. 3A). In this mode the time intervals of well pronounced population spikes are alternated by intervals of asynchronous dynamics. Let us now study such a behavior in more detail.

Figure 5A shows three raster plots of spiking activity taken in laminar (synchronous) and turbulent (asynchronous) phases during intermittency. In a laminar phase we observe rhythmic, stimulus induced, firing of population spikes. However, the firing synchronization is less pronounced than in the case of full synchronization (compare to Fig. 1A). Under a turbulent phase some stimulus event may not trigger population spikes. This can happen when in the network there appears an internal patch-type excitation that “destroys” the wave induced by the stimulus (see below). Transitions between laminar and turbulent phases can occur gradually or through a steep change in the frequency of population spikes (Fig. 5B). We then check the global characteristics of the network. Under intermittency the radial and tangential couplings do not suffer significant changes (Fig. 5C), as it also happens under full synchronization (compare to Fig. 1D). However, now the centrifugal index exhibits strong oscillations. These oscillations correlate with the oscillations of the frequency index (compare Figs. 5B and 5C). Thus, changes in the network behavior are accompanied by structural changes in the network architecture. Moreover, the determining factor is the modulation of centrifugal couplings.

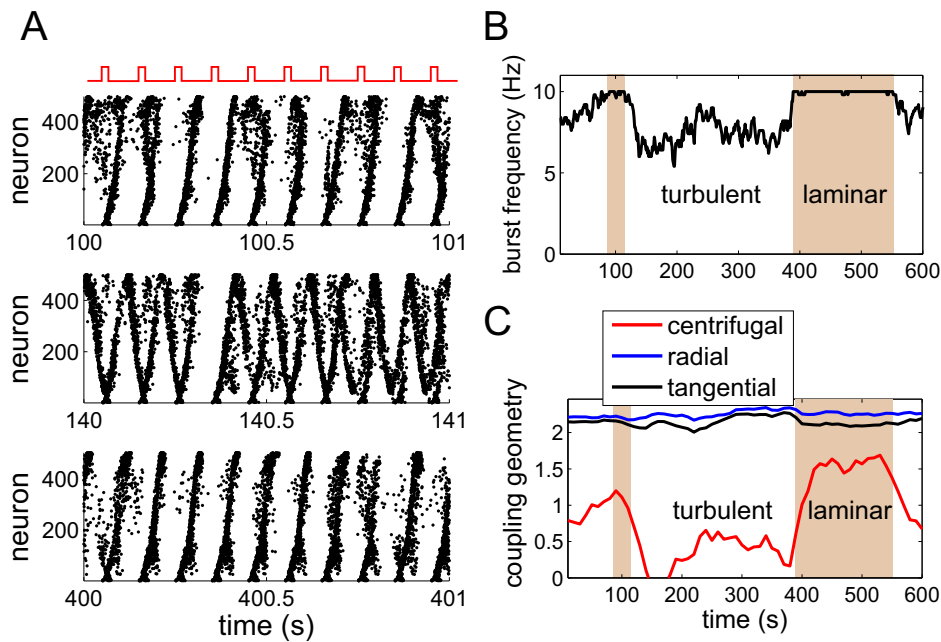


FIGURE 5. Intermittent synchronization of population spikes with external stimulus. A) Examples of raster plots for laminar (top and bottom) and turbulent (middle) phases. B) Evolution of the frequency of population spikes. Two epochs of laminar phases are marked by shaded color. C) Evolution of the structural characteristics of the network couplings.

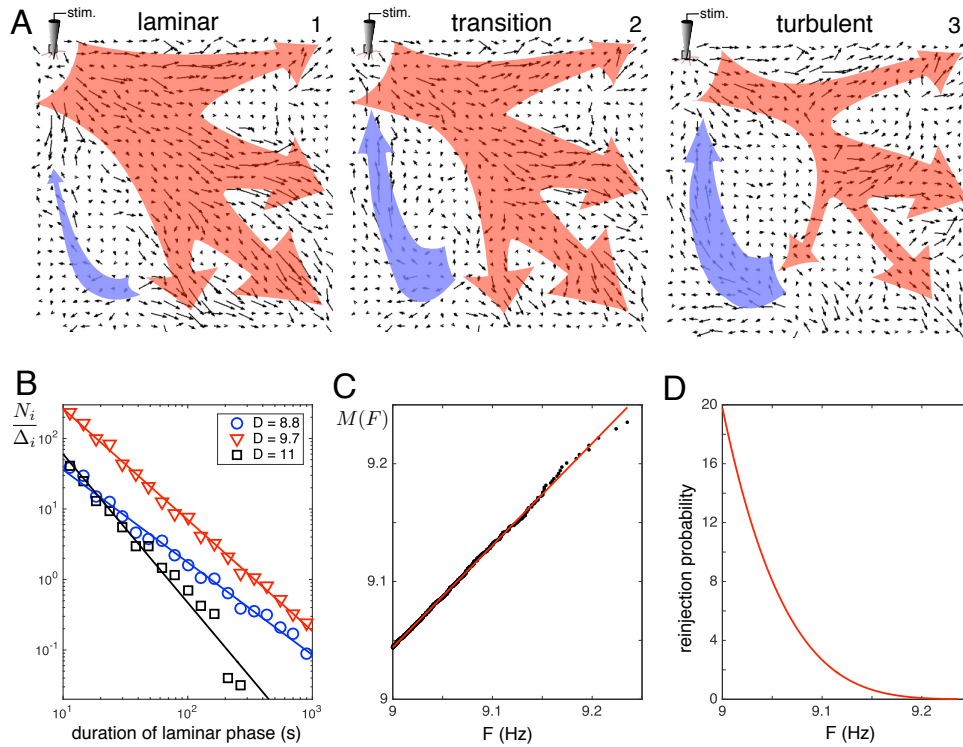


FIGURE 6. Dynamical and statistical characteristics of intermittent synchronization. A) Vector fields of the couplings (black arrows) and global directions of propagation of excitations for three time instants: in laminar (synchronous) phase (panel 1), transition from laminar to turbulent phase (panel 2), and in turbulent phase (panel 3). B) Distribution of duration of laminar (synchronous) phases under intermittent synchronization of population spikes for different values of the noise intensity. C) Fitting data function (5.2) by a straight line. D) Experimentally identified reinjection probability density determining how the network enters the laminar phase ($D = 9.7$).

To get insight on the dynamical and statistical properties of the intermittent synchronization, we first draw three maps of the vector field describing the network couplings: i) in laminar phase, ii) at transition from synchronous to asynchronous phase, and iii) in turbulent phase (Fig. 6A). In laminar phase the coupling structure facilitates propagation of excitation from the stimulus location (red arrows starting from the upper-left corner) to practically all regions in the network. This in turn promotes population spikes time locked to the stimulus. However, there is a region in the network where the direction of couplings is centripetal (Fig. 6A, panel 1, blue arrow). This direction is potentiated by STDP and at certain time it becomes strong enough to compete with the stimulus induced excitation (Fig. 6A, panel 2). Then, instead of synchronous spiking we observe propagation of spike patches in a loop (Fig. 6A, panel 3). These patches cover relatively small number of neurons and due to cyclic motion the network leaves the synchronous mode. Due to relatively low synchrony between neurons, the coupling strength first become small, but then the stimulus shapes again centrifugal couplings and the process repeats again.

Let us now study the statistical properties of the observed intermittent behavior. We divided each simulation trace (2×10^6 s long) into laminar and turbulent time intervals (Fig. 5B). We then calculated the number of laminar intervals, N_i , of the lengths falling within the interval $\Delta_i = (l_{i+1}, l_i]$, where the interval edges, l_i , were spaced logarithmically. Figure 6B shows the distribution of the relative number of

laminar phases, N_i/Δ_i , for three different values of the noise strength. In all cases the distribution follows a power law, thus we can conclude that the probability density function (pdf) of the length of laminar phases also follows a power law

$$p \propto l^k \quad (5.1)$$

The exponent k decreases with the noise strength ($k = -1.31, -1.58, \text{ and } -2.11$ for $D = 8.8, 9.7, \text{ and } 11$, respectively). Thus, for low noise intensities the pdf has longer tail. Besides, the number of laminar intervals reaches maximum for an intermediate noise intensity. In other words, we observe a kind of stochastic resonance within intermittency.

An important characteristic of intermittency is how trajectories are reinjected from the turbulent to laminar phase. The duration of laminar phase depends on how close the system enters to stationary but unstable laminar network state. Earlier we have shown that experimental data can be fitted to a model of intermittency by constructing the following function [9]:

$$M(F) = \frac{1}{j} \sum_{i=1}^j F_i, \quad F \in (F_{j-1}, F_j], \quad F_j \leq F_{j+1} \quad (5.2)$$

where F_i are the ordered values of the frequency of population spikes recorded at the beginning of each laminar phase (at reinjections). For a wide class of models exhibiting type-II and type-III intermittencies $M(F)$ follows the linear law:

$$M(F) = \begin{cases} m(F - \hat{F}) + \hat{F}, & \text{if } F \in [F_c, \hat{F}] \\ 0 & \text{otherwise} \end{cases} \quad (5.3)$$

where $m \in (0, 1)$ is a free parameter determining the reinjection probability distribution, $F_c = 9$ Hz and \hat{F} are the lower and upper boundaries of reinjection, respectively.

We thus evaluated the function (5.2) and fitted the experimental data by the straight line (5.3) (Fig. 6C). This allowed estimating the slope $m = 0.866$ and obtaining the reinjection probability distribution [9]:

$$\phi(F) = \begin{cases} A(\hat{F} - F)^\alpha, & \text{if } F \in [F_c, \hat{F}] \\ 0 & \text{otherwise} \end{cases} \quad (5.4)$$

where A is the scaling constant and $\alpha = \frac{2m-1}{1-m}$. In our case $\alpha = 4.93$, which corresponds to a rather steep descend of the reinjection probability far enough from the classical case (Fig. 6D). We notice that the exponent α does not vary much in a relatively large range of the noise intensity where an intermittent behavior is observed ($\alpha = 5.49$ and 4.73 for $D = 8.8$ and 11 , respectively). Thus, the intermittent behavior is mostly determined by the deterministic properties of the network.

6. Discussion

Last decades have shown an increasing interest to experimental studies of neuronal cultures. This fostered theoretical investigations of realistic models resembling the most prominent properties of experimental preparations. In this work we have studied a mathematical model of cortical-like neurons arbitrary distributed on a (1.2×1.2) mm substrate. Each neuron makes synaptic contacts with several target neurons from its neighborhood. Then the mean connectivity parameter (the vertex order) can be varied from 14 to 80, which allowed modeling the network behavior of different cultures from rather young to matured. The model was considered in the presence of noise simulating random perturbations affecting real neuronal cultures. An STDP mechanism of learning has been used for simulating the process of shaping the network structure under spontaneous and stimulus induced firing. We then have studied how an external periodic stimulus can drive the network and impose anatomical structure and global function as generation of a population spike.

We have shown that a local periodic stimulation supplied at a corner of the culture can rebuild synaptic couplings through the unsupervised STDP learning. Then the network behavior eventually switches from

a turbulent-like asynchronous spiking to an ordered signaling through generation of a population spike in response to each stimulus pulse. In terms of the coupling structure such an adaptation means convergence to a relatively stable (no significant changes) pattern, which can be treated as an optimal state. Such a state facilitates propagation of waves of excitation outwards from the stimulus location. Thus, population spike signaling occurs through traveling waves propagating in the neuronal culture. This requires specific network structure with dominating local couplings radially directed from the stimulus location. We thus studied the coupling geometry by introducing radial, tangential, and centrifugal indexes. The calculation have shown that in average the radial and tangential indexes do not change in time, while the centrifugal coefficient strongly increases. Since the radial index stays unchanged we can also conclude that the centripetal couplings decrease. Thus, the coupling structure becomes centrifugal, which promotes traveling waves covering all the network and hence generating a population spike. We note that such an emergent function can be useful for driving robots [6]. It is basic for generation of compact cognitive maps [34,35].

Interestingly, an uncorrelated noise of intermediate intensity can effectively catalyze the correlated firing of neurons, which, through STDP, allows shaping the architecture of synaptic couplings in the network. We then have found a phenomenon of stochastic resonance acting on the interneuron couplings. At a resonant noise level the network is able to rebuild itself and to generate population spikes in response to external stimulus. Thus, noise serves as an active substrate that helps optimizing the synaptic architecture.

Another surprising feature was the role of the connectivity index, i.e., the mean order of the vertices in neuronal graph. We have shown that highly connected networks with rather random connectivity patterns are propitious to synchronization. In terms of *in vitro* dissociated cultures, our model predicts an unexpected result: matured cultures with high connectivity can be easily reconfigured to achieve a population spike response, whereas younger cultures are less adaptable. The theoretical explanation of such an observation stems from the role of synaptic currents in the generation of spikes correlated with the stimulus. Our model suggests that the effect of high connectivity is similar to that of noise in stochastic resonance. It brings neurons closer to the spiking threshold and makes them “ready” to fire a postsynaptic spike as a response to incoming presynaptic spike originated by the stimulus. This in turn helps reshaping the network architecture to a centrifugal and thus transmitting spikes coherent with the stimulus.

We have also observed an intermittent synchronization of the network to periodic stimulus. At certain parameter values the network can switch between two quasi-stable states. One of them corresponds to strong synchronization and generation of population spikes time-locked with the stimulus, while the other is close to a turbulent regime. In the latter case the stimulus can only excite a part of the network and we observe random traveling patches of activity. We have shown that on a large scale this turbulent mode can be implemented through looping the couplings backwards to the stimulus location. Then the excitation circulates in the network and the time locking of population spikes to the stimulus is destroyed. This regime leads to a decreasing of couplings directed outwards the stimulus and to degrading the excitation circulating in the loop. Therefore the loop becomes less pronounced and eventually the stimulus wins again the competition until the loop will be formed again. Then the process repeats and we get new sequence of laminar (synchronous) and turbulent (asynchronous) phases in a similar way as it happens in the winner-less competition dynamics [29,36].

In conclusion, we note that synchronization of a network by a local periodic stimulus leading to population signaling can be treated as a simple form of an unsupervised and unconditional learning. We expect that the robust mechanisms of shaping the network architecture found in this work can be also effective in more complex preparations in studies of relationships between structure and function with implication to memory and learning in neural networks.

Acknowledgements. This work was supported by the Russian Science Foundation under project 15–12–10018.

References

- [1] S. Anishchenko, V.V. Astakhov, A.B. Neiman, T.E. Vadivasova, L. Schimansky-Geier. *Nonlinear dynamics of chaotic and stochastic systems*. Springer Verlag, Berlin, 2002.
- [2] D.J. Bakkum, Z.C. Chao, S.M. Potter. *Spatio-temporal electrical stimuli shape behavior of an embodied cortical network in a goal-directed learning task*. *J. Neur. Engin.*, 5 (2008), 310-323.
- [3] N. Benito, G. Martin-Vazquez, J. Makarova, V.A. Makarov, O. Herreras. *The right hippocampus leads the bilateral integration of gamma-parsed lateralized information*. *eLife*, (2016), doi: 10.7554/eLife.16658.
- [4] P. Berge, Y.Pomeau, C. Vidal. *Order within chaos*. New York: John Wiley and Sons, 1984.
- [5] A. Bulsara, P. Hanggi, F. Marchesoni, F. Moss M. Shlesinger. *Proceedings of the NATO ARW stochastic resonance in physics and biology*. *J. Stat. Phys.*, 70 (1993), 1-512.
- [6] C. Calvo, J.A. Villacorta-Atienza, V.I. Mironov, V. Gallego, V.A. Makarov. *Waves in isotropic totalistic cellular automata: Application to real-time robot navigation*. *Advan. Compl. Syst.*, 19(4) (2016), 1650012-18.
- [7] Z.C. Chao, D.J. Bakkum, D.A. Wagenaar, S.M. Potter. *Effects of random external background simulation on network synaptic stability after tetanization: a modeling study*. *Neuroinformat.*, 3(3) (2005), 263-280.
- [8] Z.C. Chao, D.J. Bakkum, S.M. Potter. *Region-specific network plasticity in simulated and living cortical networks: comparison of the center of activity trajectory (CAT) with other statistics*. *J. Neur. Engin.*, 4 (2007), 294-308.
- [9] E. Del Rio, S. Elaskar, V.A. Makarov. *Theory of intermittency applied to classical pathological cases*. *Chaos*, 23 (2013), 033112.
- [10] T.B. DeMarse, D.A. Wagenaar, A.W. Blau, S.M. Potter. *The neurally controlled animat: biological brains acting with simulated bodies*. *Autonom. Robots*, 11 (2001), 305-310.
- [11] T. Gritsun, J. le Feber, J. Stegenga. *Network bursts in cortical cultures are best simulated using pacemaker neurons and adaptive synapses*. *Biol. Cybern.*, 102 (2010), 293-310.
- [12] T. Gritsun, J. le Feber, W.L.C. Rutten. *Growth dynamics explain the development of spatiotemporal burst activity of young cultured neuronal networks in detail*. *PLoS ONE*, 7(9) (2012), e43352.
- [13] G.W. Gross, J.M. Kowalski. *Origins of activity patterns in self-organizing neuronal networks in vitro*. *J. Intell. Mater. Syst. Struct.*, 10(7) (1999), 558-564.
- [14] R. Gutig, R. Aharonov, S. Rotter, H. Sompolinsky. *Learning input correlations through nonlinear temporally asymmetric Hebbian plasticity*. *J. Neurosci.*, 23 (2003), 3697-3714.
- [15] O. Herreras, J. Makarova, V.A. Makarov. *New uses of LFPs: pathway-specific threads obtained through spatial discrimination*. *Neuroscience*, 310 (2015), 486-503.
- [16] A.E. Hramov, A.A. Koronovskii, O.I. Moskalenko, M.O. Zhuravlev, V.I. Ponomarenko, M.D. Prokhorov. *Intermittency of intermittencies*. *Chaos*, 23(3) (2013), 033129.
- [17] E.M. Izhikevich. *Simple model of spiking neurons*. *IEEE Trans. Neur. Netw.*, 14 (2003), 1569-1572.
- [18] F. Kawasaki, M. Stiber. *A simple model of cortical culture growth: burst property dependence on network composition and activity*. *Biol. Cybern.*, 108(4) (2014), 423-443.
- [19] S. Lobov, A. Simonov, I. Kastalskiy, V. Kazantsev. *Network response synchronization enhanced by synaptic plasticity*. *Eur. Phys. J. Special Topics*, 225(1) (2016), 29-39.
- [20] E. Maeda, H.P.C. Robinson, A. Kawana. *The mechanisms of generation and propagation of synchronized bursting in developing networks of cortical neurons*. *J. Neurosci.*, 15(10) (1995), 6834-6845.
- [21] J. Makarova, V.A. Makarov, O. Herreras. *Generation of sustained field potentials by gradients of polarization within single neurons: a macroscopic model of spreading depression*. *J. Neurophysiol.*, 103 (2010), 2446-2457.
- [22] S. Marom, G. Shahaf. *Development, learning and memory in large random networks of cortical neurons: lessons beyond anatomy*. *Quart. Rev. Biophys.*, 35(1) (2002), 63-87.
- [23] G. Martin-Vazquez, N. Benito, V.A. Makarov, O. Herreras, J. Makarova. *Diversity of LFPs activated in different target regions by a common CA3 input*. *Cereb. Cortex*, 26(10) (2016), 4082-4100.
- [24] M.D. McDonnell and L.M. Ward. *The benefits of noise in neural systems: bridging theory and experiment*. *Nat. Rev. Neurosci.*, 12 (2011), 415-426.
- [25] A. Morrison, M. Diesmann, W. Gerstner. *Phenomenological models of synaptic plasticity based on spike timing*. *Biol. Cybern.*, 98 (2008), 459-478.
- [26] A. Pimashkin, I. Kastalskiy, A. Simonov, E. Koryagina, I. Mukhina, V. Kazantsev. *Spiking signatures of spontaneous activity bursts in hippocampal cultures*. *Front. Comput. Neurosci.*, 5 (2011), 46.
- [27] H.G. Schuster. *Deterministic Chaos: An Introduction*. in *Physik*, Weinheim, 1984.
- [28] R. Segev, Y. Shapira, M. Benveniste, E. Ben-Jacob. *Observations and modeling of synchronized bursting in two-dimensional neural networks*. *Phys. Rev. E*, 64(01) (2001), 011920.
- [29] A. Selskii, V.A. Makarov. *Synchronization of heteroclinic circuits through learning in coupled neural networks*. *Regular Chaotic Dynamics*, 21 (2016), 97-106.
- [30] G. Shahaf, D. Eytan, A. Gal, E. Kermany, V. Lyakhov, C. Zrenner, S. Marom. *Order-based representation in random networks of cortical neurons*. *PLoS Comput. Biol.*, 4(11) (2008), e1000228.
- [31] S. Song, K.D. Miller, L.F. Abbott. *Competitive Hebbian learning through spike-timing-dependent synaptic plasticity*. *Nat. Neurosci.*, 3(9) (2000), 919-926.
- [32] M. Tsodyks, K. Pawelzik, H. Markram. *Neural network with dynamic synapses*. *Neural Comput.*, 10 (1998), 821-835.
- [33] J. Van Pelt, P.S. Wolters, M.A. Corner, W.L.C. Rutten, G.J.A. Ramakers. *Long-term characterization of firing dynamics of spontaneous bursts in cultured neural networks*. *IEEE Trans. Biomed. Eng.*, 51(11) (2004), 2051-2062.

- [34] J.A. Villacorta-Atienza, C. Calvo, V.A. Makarov. *Prediction-for-CompAction: Navigation in social environments using generalized cognitive maps*. Biol. Cybern., 109(3) (2015), 307-320.
- [35] J.A. Villacorta-Atienza, V.A. Makarov. *Neural network architecture for cognitive navigation in dynamic environments*. IEEE Trans. Neur. Netw. Learn. Syst., 24(12) (2013), 2075-2087.
- [36] P. Varona, M.I. Rabinovich, A.I. Selverston, Y.I. Arshavsky. *Winnerless competition between sensory neurons generates chaos: a possible mechanism for molluscan hunting behavior*. Chaos, 12 (2002), 672-677.
- [37] D.A. Wagenaar, J. Pine, S.M. Potter. *An extremely rich repertoire of bursting patterns during the development of cortical cultures*. BMC Neurosci., 7(11) (2006).